Simulation of stationary sheet metal cutting processes

H.H. Wisselink and J. Huétink
Fac. Mechanical Engineering, University of Twente, Enschede, The Netherlands

ABSTRACT: In stationary sheet metal cutting processes, like guillotining and slitting, the sheet is cut progressively from one end to the other. This in contrary with transient processes (blanking) where the sheet is cut at once. Where transient shearing processes can be modelled in 2-D (plain strain or axisymm.), stationary shearing processes have to be modelled in 3-D. For the calculation of the steady state of the guillotining process a 3-D finite element model is developed. Also plane strain shearing simulations are performed. The Arbitrary Lagrangian Eulerian method is used for all simulations. The results of both cases are presented and compared with each other.

1 INTRODUCTION

A guillotine-type shear (Figure 1) has two straight blades. The shearing angle α is the angle between the upper and lower blade. When the upper blade is inclined ($\alpha > 0°$) the sheet is cut progressively from one end to the other, which is a stationary process. In case of parallel blades ($\alpha = 0°$) the sheet is cut at once and the process is transient.

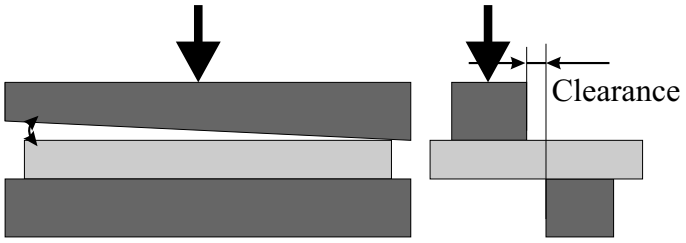

Figure 1: Guillotining

While the nett result for the sheared edge is the same in both cases, there are some differences between the two. The force required to cut the sheet is decreasing with increasing shearing angle, since only part of the sheet is cut at a moment. But also the quality of the sheared products is deteriating with increasing shearing angle α. The sheet has to bend to conform to the inclination of the blade. This causes some irregularities in the sheet, especially for small off-cuts (Figure 2). Therefore a compromise has to be made between required force and the quality of the cut sheet. In practice the shearing angle varies between 1°–3°.

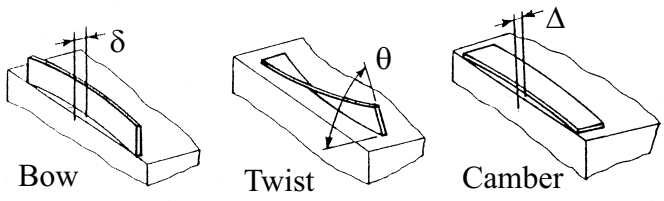

Figure 2: irregularities after cutting

The sheet undergoes elastic and plastic deformation when the upper blade is forced down. After penetrating to a specific part of the thickness of the sheet the unpenetrated part fractures and the cut is completed. These phases occur sequently in orthogonal shearing. Guillotining however is a steady state composite of these phases. The size of the different phases depends on the material characteristics, clearance and blade geometry.

The knowledge of shearing processes is mainly empirical (Sperling 1968). The objective of this study is to gain more insight in these processes. Therefore a finite element model is developed by which the influence of the parameters on the shearing process can be studied. The results should contribute to a better process controll.

2 MODELLING SHEARING PROCESSES

For a complete simulation of the shearing process all phases should be described properly. This means that large deformations with history dependent material behaviour, contact and ductile fracture must be incorporated in the model.

2.1 *Large deformations*

Eulerian formulations are capable of handling large material deformations, but are less suited for the description of history dependent material behaviour and the movement of free surfaces. In Lagrangian formulations path dependent material properties and the movement of free surfaces can easily be described, but this formulation can fail in simulating forming processes when the element grid becomes too much distorted. Therefore the Arbitrary Lagrangian Eulerian formulation (ALE, discussed in Section 3) is used. With such a formulation it is possible to handle history dependent material behaviour, to follow free surfaces and to keep the mesh regular.

In the 2D transient shearing simulations (plane strain or axisymmetric) reported in literature remeshing (Morançay et al. 1997), or a combination of remeshing and the ALE method (Brokken et al. 1997) is used to avoid excessive element deformation. For the transient simulations presented in this paper only the ALE method is used, which in this case can be seen as remeshing with a constant number of elements and mesh topology. Even though the ALE method is suited for large deformations, it is difficult to keep a regular mesh for large geometry changes, as is the case in shearing. This limits our 2D calculations to penetrations of about half the sheet thickness.

The simulations of 3D stationary processes with the ALE method do not have this drawback when the initial geometry is chosen close enough to the expected final geometry. This type of calculation has mainly Eulerian characteristics with the possibility to follow free surfaces.

2.2 *Ductile fracture*

The sheets are finally seperated by a ductile fracture process. Again there is a difference between stationairy and transient shearing processes. In the transient case no cracks are initially present. After some punch penetration a crack initiates, which will subsequently grow leading to complete separation. Some different approaches for the simulation of ductile failure in shearing have been presented by (Bezzina and Saanouni 1997),(Morançay et al. 1997), (Brokken et al. 1997) and (Taupin et al. 1996).

In the stationary case the crack growth is stable and an inital crack front can be modelled. The crack front is a free surface, which position depends on some fracture criterion. With the ALE method and a fracture model it should be possible to adapt the crack front from a initial guess to it's steady state position. However this phase is not yet incorporated in our model.

3 ALE METHOD

The ALE method is implemented in DiekA, a finite element code developed at the University of Twente. In the ALE formulation mesh and material displacements are independent. First an Updated Lagrangian step is done to calculate the material displacements. Next the grid displacements are determined using the strategies in Section 3.1. When the new mesh is known the history dependent quantities are transferred to this mesh. This is a convective displacement over the difference between material and grid displacement (Section 3.2).

3.1 *Definition of a new mesh*

When determinating the new positions of the nodes, two kind of nodes can be distinguished. Nodes on the surface, which should remain on the surface and internal nodes which can moved freely in the material as long as a good element shape is preserved. In the 3-D calculations presented in this paper, internal nodes are spatially fixed.

The geometry is meshed in such a way that the initial mesh on the surfaces is regular. During the simulation the surface mesh is kept regular. The grid is fixed in flow direction (x-direction). Perpendicular to the flow direction (in the yz-plane) the grid is following the free surface.

Determining new nodal positions of surface points can be seen as a convection problem. This convection is done in two steps. First convection along a gridline in the flow direction is carried out. This is illustrated in Figure 3. The x-coordinate of a node after the Lagrangian step is x_i^n. The new x-coordinate is x_i^{n+1}, which is the same as the x-coordinate before the Lagrangian step. y^n are the known y-coordinates after the Lagrangian step. The new y-coordinate y^{n+1} at x_i^{n+1} has to be calculated. For the convection a second order Lax-Wendroff scheme with van Leer limiters is chosen.

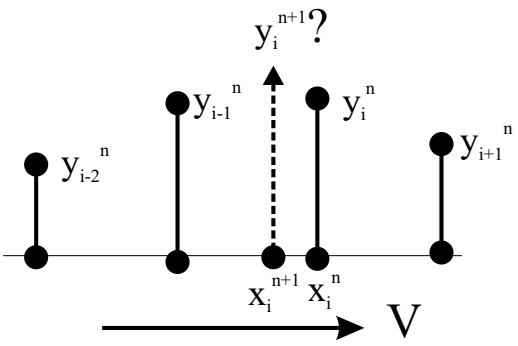

Figure 3: Convection of nodal coordinates

This second order scheme is stable and shows no oscillations (Akkerman et al. 1995),(Helm et al. 1998).

The new y-coordinate y_i^{n+1} is then

$$y_i^{n+1} = y_i^n - C\left(y_i^n - y_{i-1}^n\right) - \frac{1}{2}C(1-C)\left[\psi(r_{i+1/2})(y_{i+1}^n - y_i^n) - \psi(r_{i-1/2})(y_i^n - y_{i-1}^n)\right] \quad (1)$$

Where C is the Courant number which is a measure for the relative displacement between the material and the mesh. l_e is a characteristic elementlength.

$$C = \frac{V\Delta t}{l_e} = \frac{\Delta x}{l_e} \quad (2)$$

The van Leer limiter $\psi(r)$ stabilizes the Lax-Wendroff scheme when the gradients are large.

$$r_{i+1/2} = \frac{y_i^n - y_{i-1}^n}{y_{i+1}^n - y_i^n}; \quad r_{i-1/2} = \frac{y_{i-1}^n - y_{i-2}^n}{y_i^n - y_{i-1}^n} \quad (3)$$

$$\psi(r) = \frac{r + |r|}{1 + |r|} \quad (4)$$

The same procedure is applied to calculate the new z-coordinate

The application of the scheme is illustrated with a test problem. The initial mesh is shown in Figure 4. A "bubble" is moving in x-direction with a velocity V. The nodes on the upper surface are adapted with the described scheme. All other nodes are spatially fixed. In Figure 5 the results are shown after some steps. From this can be concluded that the scheme used is stable but also shows some diffusion.

After the convection in flow-direction for all nodes is completed, a second convection step perpendicular on the flow direction (in the yz-plane)

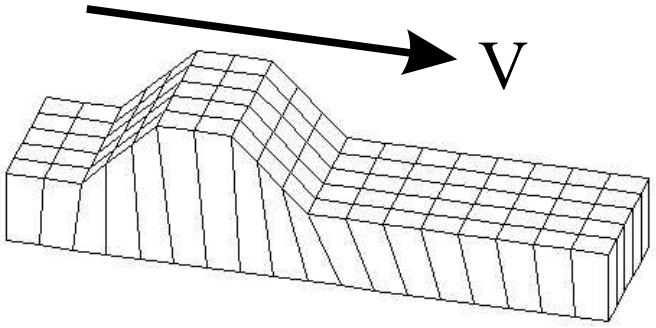

Figure 4: Initial mesh of test problem

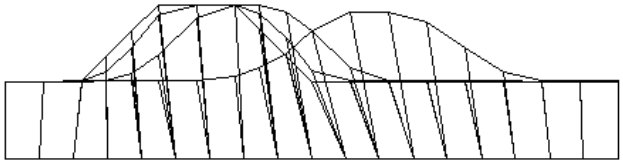

Figure 5: Geometry of test problem after 0/25/50/100 steps

will be done. Herein the nodes are kept regularly spaced. The Courant number and direction of convection are determinated from the material displacements in the lagrangian step. Again convection is done with the limited Lax-Wendroff scheme.

For the 2-D simulations a more sophisticated mesh management procedure is available in DiekA, based on (Ponthot 1989). His ideas can also be used to improve the quality of the mesh in the 3-D case.

3.2 *Transfer of state variables*

For the transfer of the history dependent quantities several procedures are available in 2-D (Stoker and Huétink 1996). The method of weighed local and global smoothing (Huétink et al. 1990), (Huétink and Helm 1992) can be used in 2- and 3-D. Therefore this method is chosen for the simulations in this paper, and is explained briefly.

The material rate of change of a material quantity f (stresses or strains) can be expressed as

$$\dot{f}^m = \frac{df}{dt}^m = \frac{\partial f}{\partial t} + \dot{\mathbf{x}}^m \cdot \overrightarrow{\nabla} f \quad (5)$$

and the rate of change in a grid point

$$\dot{f}^g = \frac{df}{dt}^g = \frac{\partial f}{\partial t} + \dot{\mathbf{x}}^g \cdot \overrightarrow{\nabla} f \quad (6)$$

$\dot{\mathbf{x}}^m$ and $\dot{\mathbf{x}}^g$ are respectively the material and grid

velocity. Combining (5) and (6) gives

$$\dot{f}^g = \dot{f}^m + (\dot{\mathbf{x}}^g - \dot{\mathbf{x}}^m) \cdot \overrightarrow{\nabla} f \tag{7}$$

Equation (7) implies that when the grid and material displacement are uncoupled, convection must be taken into account. The value of f in a grid point $\mathbf{x}^g$ can be approximated using an incremental form of (7)

$$f(\mathbf{x}^g + \Delta\mathbf{x}^g, t + \Delta t) = \Delta f^m + f(\mathbf{x}^g, t) + (\Delta\mathbf{x}^g - \Delta\mathbf{x}^m) \cdot \overrightarrow{\nabla} f \tag{8}$$

Which can be seen as a spatial Taylor series expansion of

$$f(\mathbf{x}^g + \Delta\mathbf{x}^g, t + \Delta t) = \Delta f^m + f(\mathbf{x}^g + \Delta\mathbf{x}^g - \Delta\mathbf{x}^m, t) \tag{9}$$

To obtain the gradient $\overrightarrow{\nabla} f$, a continuous field is constructed by extrapolating the integration point values to the nodes. Averaging nodal point values (f^N) and interpolating by Ψ^N gives a continuous field f^* which is different from the initial internal element values f.

$$f^* = \Psi^N f^N \tag{10}$$

$$\overrightarrow{\nabla} f^* = \overrightarrow{\nabla} \Psi^N f^N \tag{11}$$

Convection with (8) and (11) is unstable. Another possibility to calculate the convection is to use the smoothed continuous function f^* and (9).

$$f(\mathbf{x}^g + \Delta\mathbf{x}^g, t + \Delta t) = \Delta f^m + \Psi^N(\mathbf{x}^g + \Delta\mathbf{x}^g - \Delta\mathbf{x}^m, t) f^N \tag{12}$$

This method is stable but also very diffusive. Therefore both methods are combined and the convection is done with a weighed sum of (8) and (12).

$$f(x^g + \Delta x^g, t + \Delta t) = \Delta f^m + (1-\alpha)\left[f(x^g, t) + (\Delta x^g - \Delta x^m) \cdot \overrightarrow{\nabla} \Psi^N f^N\right] + \alpha\left[\Psi^N(x^g + \Delta x^g - \Delta x^m, t) f^N\right] \tag{13}$$

The weight factor α is taken as a function of the Courant number and from numerical studies a reasonable range appeared to be

$$C \leq \alpha(C) \leq 2C \tag{14}$$

This means that for large Courant numbers more diffusion is added than for small Courant numbers. For $C = 0$ (No convection) the method is exactly the same as the Updated Lagrangian formulation.

4 SIMULATION RESULTS

Results of a 2D plane strain simulation and a 3D stationary guillotining simulation are presented in this Section. The only difference between these simulations is the shearing angle, which is 5.7° in guillotining and 0° in plain strain.

An elastic-plastic material model is used, with a Von Mises yield criterion for the plastic flow. Hardening is described with a extended Nadai formula.

$$\sigma_y = \sigma_0 + C(\varepsilon_0 + \varepsilon^p)^n \tag{15}$$

For the contact with the rigid tools a penalty method is applied (Huétink et al. 1990). The horizontal movement of the sheet perpendicular to the flow direction, is suppressed at the boundaries.

Table 1: Tool and Sheet geometries

sheet thickness	1 mm
sheet width	4 mm
radii	0.01 mm
clearance	10%
friction coefficient	0.2

Table 2: Material properties

ε_0	$7.1 \cdot 10^{-3}$
σ_0	15.7 MPa
C	565.3 Mpa
n	0.2589
E-modulus	206 MPa
ν	0.3

In Figure 6 the element meshes of the plane strain simulation are shown. With the ALE method bad shaped elements are avoided and the elements are kept small around the tool radii, where the strains and stresses are large.

Figure 7(a) gives the initial mesh for the stationary simulation. The material flows from the left to the right through the mesh. The tools (not drawn) are moving with the same speed as the material flows in. The position of the nodes on the surface is adapted every step with the algorithm of Section 3.1. The calculation is continued until a steady state is reached. The difference between the initial and steady state geometry is best seen in the process zone.

The results from the plain strain and stationary calculations for a cross-section with a tool penetration of 50% sheet thickness are compared. In

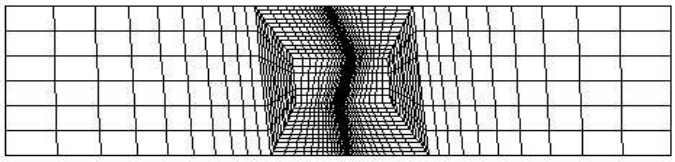

(a) Initial mesh

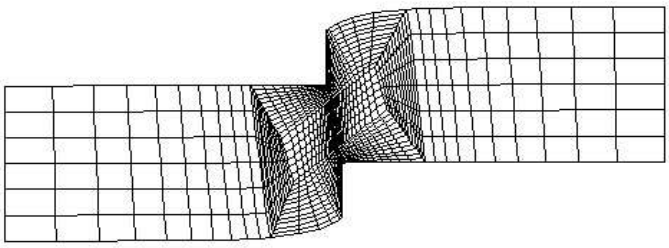

(b) 50% penetration

Figure 6: Plane strain meshes

Figures 8 and 9 the equivalent plastic strain and hydrostatic pressure are given. The trends in the graphs are the same. Between the tool tips an area with large strain and hydrostatic tension has developed. The differences in stress and strain between the plane strain and the stationary case, can be explained by the difference in mesh density. In the plain strain simulation 1254 4-node elements are used. The total number of 8-node elements in the 3-D stationary simulation is 5088, which is 318 elements per cross-section. So the 3-D mesh is about 4 times as coarse than the 2-D mesh. 3-D calculations with finer meshes are not carried out because it takes, even with an iterative solver, much time to solve.

The influence of the shearing angle can be illustrated with Figure 10. The stresses in flow-direction form two bending moments, which bend the sheet. These bending stresses are sensitive for the applied boundary conditions. The way the cut-off sheet is clamped influences the irregularities in Figure 2 (Murakawa and Yan 1997). In practice the cut-off part is clamped much less than in our simulation and the sheet will bend and twist much more. This means for the calculation that it is not sufficient anymore to keep the internal nodes spatially fixed.

5 CONCLUSIONS

From the presented results can be concluded that the ALE method is very suitable for the simulation of stationary shearing processes. Free surfaces can be followed with the procedure from Section 3.1. A

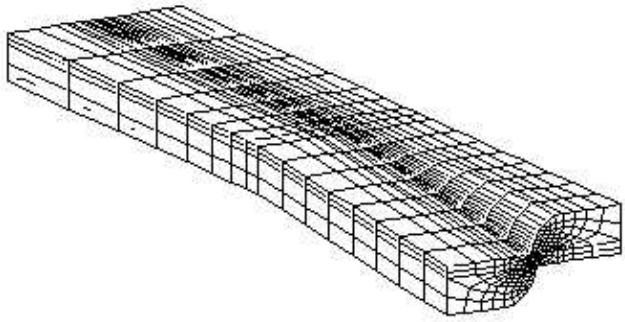

(a) Initial mesh

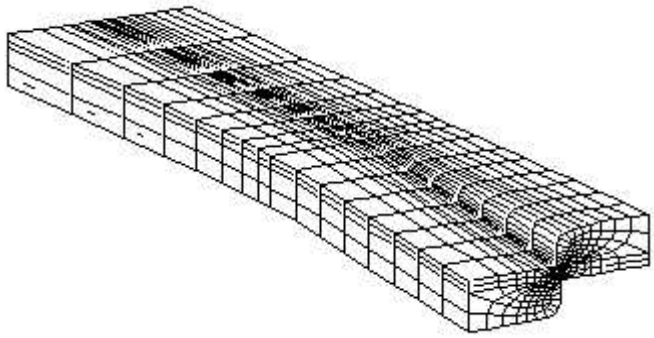

(b) Steady state mesh

Figure 7: 3-D meshes; 75% penetration

method for moving internal nodes should be implemented to obtain a better internal element mesh and to handle other (less constrained) boundary conditions. For a complete simulation an algorithm is needed that describes ductile failure.

Since 3-D calculations consume much more computer time than plane strain calculations it should be investigated whether the influence of some parameters can be studied as good in plane strain as in full 3-D.

REFERENCES

Akkerman, R., J. Huétink, and P. N. v. d. Helm (1995). Finite elements and volumes in a euler-lagrange formulation -artificial dissipation versus limited flux schemes. In D. Owen, E. Onate, and E. Hinton (Eds.), *Computational Plasticity, Fund. and Appl.*, pp. 2307–2318.

Bezzina, S. and K. Saanouni (1997). Computational procedures for finite strain elastoplasticity with damage: application for sheet cutting. In D. Owen, E. Onate, and E. Hinton (Eds.), *Computational Plasticity, Fund. and Appl.*, pp. 611–618.

Brokken, D., A. Goijaerts, W. Brekelmans,

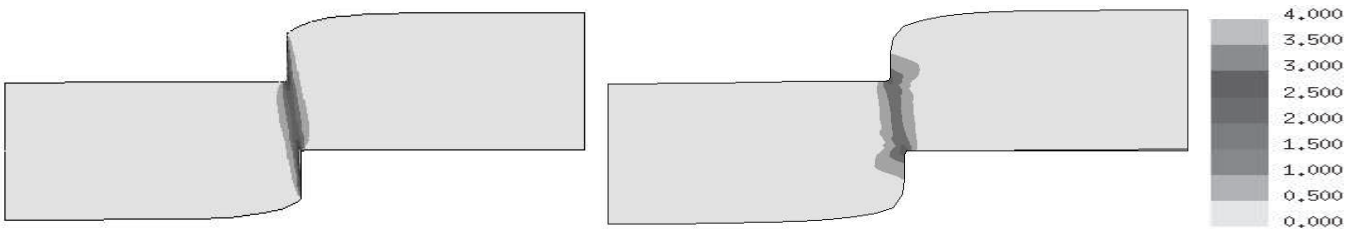

(a) plane strain (b) stationary

Figure 8: equivalent plastic strain at 50% penetration

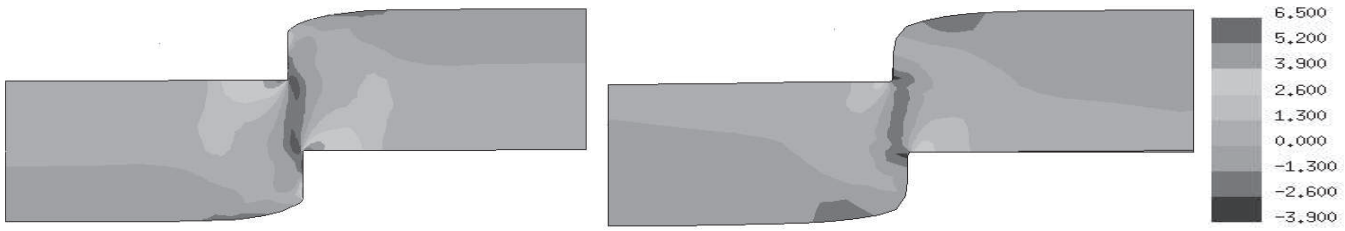

(a) plane strain (b) stationary

Figure 9: hydrostatic pressure ($*100MPa$) at 50% penetration

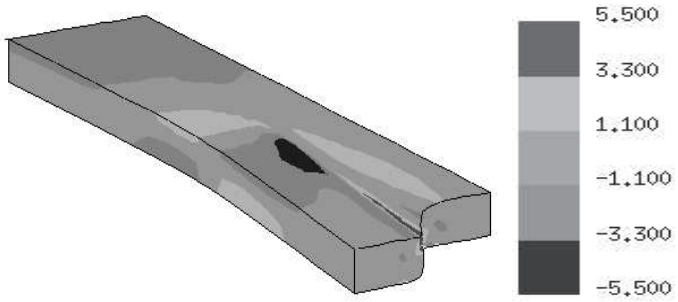

Figure 10: bending stresses: $\sigma_{xx}(*100MPa)$

C. Oomens, and F. Baaijens (1997). Modelling of the blanking process. In D. Owen, E. Onate, and E. Hinton (Eds.), *Computational Plasticity, Fund. and Appl.*, pp. 1417–1424.

Helm, P. N. v. d., J. Huétink, and R. Akkerman (1998). Comparison of artificial dissipation and limited flux schemes in Arbitrary Lagrangian Eulerian finite element formulations. *Int. J. Num. Meth. Eng. 41*(6), 1057–1076.

Huétink, J. and P. N. v. d. Helm (1992). On Euler–Lagrange finite element formulation in forming and fluid problems. In J. L. Chenot (Ed.), *Num. Methods in Ind. Form. Processes, Proc. NUMIFORM '92*. Balkema, Rotterdam.

Huétink, J., P. T. Vreede, and J. v. d. Lugt (1990). Progress in mixed Eulerian–Lagrangian finite element simulation of forming processes. *Int. J. Num. Meth. Eng. 30*, 1441–1457.

Morançay, L., H. Homsi, and J. Roelandt (1997). Application of remeshing technics to the simulation of metal cutting by punching. In D. Owen, E. Onate, and E. Hinton (Eds.), *Computational Plasticity, Fund. and Appl.*, pp. 1065–1070.

Murakawa, M. and L. Yan (1997). Precision cutting of sheets by means of a new shear based on rolling motion. *J. Mat. Proc. Tech. 66*, 232–239.

Ponthot, J. P. (1989). Efficient mesh management in Eulerian–Lagrangian method for large deformation analysis. In E. G. Thompson, R. D. Wood, O. C. Zienkiewicz, and A. Samuelsson (Eds.), *Num. Methods in Ind. Form. Processes, Proc. NUMIFORM '89*, pp. 203–210. Balkema, Rotterdam.

Sperling, H. (1968). Die schnittqualität bei Tafelscheren. *Blech 15*(4), 164–169. in German.

Stoker, H. and J. Huétink (1996). The Arbitrary Lagrangian-Eulerian method in large deformation problems. In *ECCOMASS 96*, pp. 184–189. John Wiley & Sons, Ltd.

Taupin, E., J. Breitling, W. Wu, and T. Altan (1996). Material fracture and burr formation in blanking, results of fem simulations and comparison with experiments. *J. Mat. Proc. Tech. 59*, 68–78.